


Cell-free osteoarthritis treatment with dual-engineered chondrocyte-targeted extracellular vesicles derived from mechanical loading primed mesenchymal stem cells

Peng Wang^{1,2*}, Haiyue Zhao^{2,3*}, Wei Chen^{2*}, Yuhui Guo², Shuo Zhang^{2,3}, Xin Xing², Shuai Yang^{2,3}, Fengkun Wang^{2,3}, Juan Wang², Zengwu Shao¹ and Yingze Zhang^{1,2} 

Abstract

Osteoarthritis (OA) is an age-related chronic inflammatory disease, predominantly characterized by chondrocyte senescence and extracellular matrix (ECM) degradation. Although mesenchymal stem cells (MSCs) derived extracellular vesicles (EVs) are promising for promoting cartilage regeneration, their clinical application is limited by inconsistent therapeutic effects and insufficient targeting capabilities. Mechanical loading shows potential to optimize MSC-EVs for OA treatment, while the underlying mechanism is not clear. In this study, EVs derived from mechanical loading-primed MSCs (ML-EVs) demonstrate prominent efficacy in maintaining ECM homeostasis and relieving chondrocyte senescence, thereby mitigating OA. Subsequent miRNA sequencing reveals that ML-EVs exert their effects by delivering miR-27b-3p, which targets ROR1 mRNA in chondrocytes and suppresses downstream NF- κ B pathways. By modulating the ROR1/NF- κ B axis, miR-27b-3p effectively restrains ECM degradation and chondrocyte senescence. To optimize therapeutic efficacy of EVs, miR-27b-3p is overexpressed within EVs (miR^{OE}-EVs), and a chondrocyte-targeted peptide (CTP) is conjugated to their surface, thereby constructing dual-engineered chondrocyte-targeted EVs (CTP/miR^{OE}-EVs). CTP/miR^{OE}-EVs exhibit excellent ability to specifically target cartilage and ameliorate OA pathology. In conclusion, this study underscores the critical role of mechanical loading in augmenting effectiveness of EVs in mitigating OA and introduces dual-engineered EVs that specifically target chondrocytes, providing a promising therapeutic strategy for OA.

Keywords

Osteoarthritis, extracellular vesicles, mechanical loading, mesenchymal stem cells, chondrocyte-targeted peptide

Date received: 8 October 2024; accepted: 23 December 2024

¹Department of Orthopaedics, Union Hospital, Tongji Medical College, Huazhong University of Science and Technology, Wuhan, China

²Department of Orthopaedic Surgery, The Third Hospital of Hebei Medical University, Shijiazhuang, China

³School of Medicine, Nankai University, Tianjin, China

*These authors contributed equally to this work.

Corresponding authors:

Yingze Zhang, Department of Orthopaedics, Union Hospital, Tongji Medical College, Huazhong University of Science and Technology, No. 1277 Jiefang Avenue, Wuhan 430022, China.
Email: yzling_liu@163.com

Zengwu Shao, Department of Orthopaedics, Union Hospital, Tongji Medical College, Huazhong University of Science and Technology, No. 1277 Jiefang Avenue, Wuhan 430022, China.

Email: szwpro@163.com

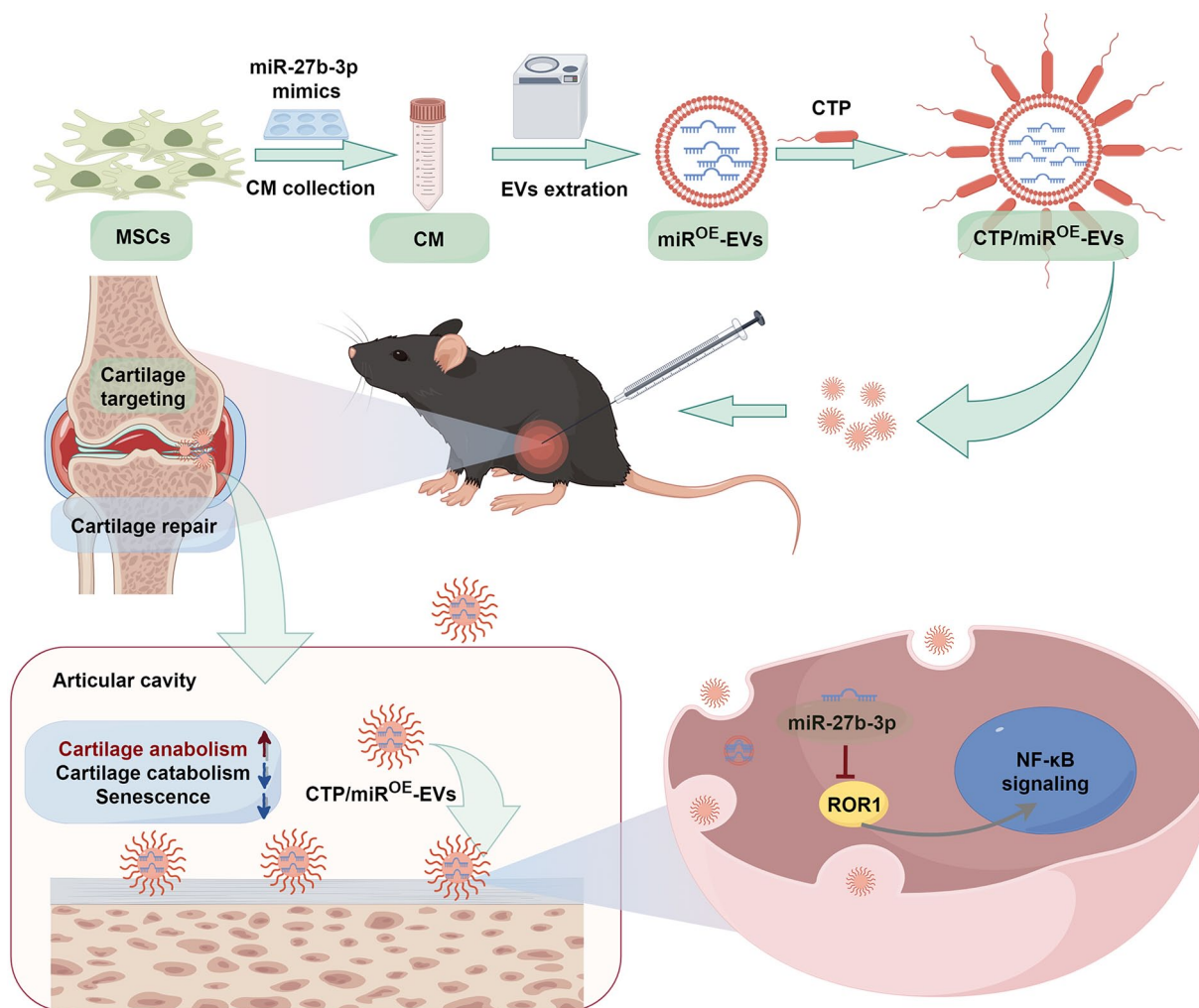
Juan Wang, Department of Orthopaedic Surgery, The Third Hospital of Hebei Medical University, No. 139 Ziqiang Road, Shijiazhuang 050051, China.

Email: wang_heb3y@163.com



Graphical abstract

Schematic diagram of the development of dual-engineered EVs with overexpressed miR-27b-3p and chondrocyte-targeting property toward a cell-free OA treatment



Introduction

Osteoarthritis (OA), a common degenerative joint disorder associated with aging, is the primary contributor to disability in elderly individuals and significantly impacts quality of life.¹ The current treatment options for OA involve non-pharmacological interventions, pain management, and surgical options, but effective disease-modifying therapies are lacking.² The primary pathophysiological mechanism of OA involves multifaceted interaction among inflammation, cellular senescence, and degradation of the extracellular matrix (ECM), leading to disrupted cartilage homeostasis.³ The quantity of senescent chondrocytes escalated in tandem with the progression of OA, as the senescence-associated secretory phenotype (SASP) produced by these cells further promotes senescence of chondrocytes and cartilage breakdown.^{4,5} Since chondrocytes are the primary cells responsible for maintaining cartilage

homeostasis, relieving chondrocyte senescence is promising for alleviating OA pathogenesis.^{6,7}

Mesenchymal stem cells (MSCs) have been utilized in the clinical management of OA because of their ability to facilitate cartilage regeneration.⁸ Nevertheless, the extensive clinical use of MSCs has been limited by challenges such as poor transplant survival, high cost, and uncertain long-term efficacy and safety.^{9,10} Recently, extracellular vesicles (EVs) derived from MSCs (MSC-EVs) have been shown to inherit the advantages of MSCs, including promoting cellular proliferation and chondrogenic differentiation and impeding inflammation and apoptosis.^{11–13} MSC-EVs mediated treatment is characterized by low toxicity, low immunogenicity, and high engineerability.¹⁴ These EVs carry various bioactive molecules, such as nucleic acids, lipids, and proteins, in which miRNAs have been proven to contribute to therapeutic effects.¹⁵ Accumulating evidence has shown that EVs can transfer

functional miRNAs to recipient cells within the OA joint, where they can regulate target gene expression and modulate cellular responses.¹⁶ For example, miR-223, which is abundant in MSC-EVs, has been shown to maintain chondrocyte homeostasis and alleviate OA by suppressing the NLRP3/pyroptosis axis.¹⁷ Taken together, these findings indicated that MSC-EVs hold promise for cell-free therapy on alleviating OA through the delivery of miRNAs.

Although MSC-EVs demonstrate promising potential for alleviating OA, their low yield and unstable effects hinder their widespread utilization.¹⁸ In addition, owing to the complex microenvironment and lack of specific cartilage-targeting strategies, EVs may be quickly eliminated from the articular cavity, resulting in the loss of a lasting effect.^{14,19} Therefore, increasing the production of EVs and enhancing their therapeutic effects and targeting ability are crucial for their clinical application. On the one hand, to improve yield and therapeutic effects, MSCs are pretreated via various biophysical and biochemical methods, including 3D culture, hypoxic condition, cytokines, and other chemical and physical preconditioning methods.¹⁸ In particular, mechanical loading, such as extrusion or stretching, markedly enhances the release of EVs with improved cartilage regenerative potential.^{20,21} On the other hand, to enhance the targeting ability, engineering EVs are constructed through membrane surface modification and endosomal therapeutic molecule loading.¹⁴ EVs modified with a chondrocyte affinity peptide or a collagen II-targeting peptide demonstrated better therapeutic benefits for OA by specifically targeting cartilage.^{6,17} Nevertheless, the effect and underlying mechanism of mechanical loading of MSC-EVs for OA treatment remain incompletely understood.

In the present study, we found that appropriate mechanical loading preconditioning optimized the ability of EVs to maintain ECM metabolic homeostasis and alleviate chondrocyte senescence, thereby attenuating OA. Further mechanistic exploration revealed that mechanical loading increased the abundance of miR-27b-3p in EVs. By targeting ROR1 in chondrocytes, miR-27b-3p impeded the activation of downstream NF- κ B pathways, thereby maintaining ECM metabolic homeostasis and alleviating chondrocyte senescence. Next, we overexpressed miR-27b-3p in EVs and modified the engineered EVs with chondrocyte-targeted peptide (CTP) to construct a dual-targeted treatment for OA. This study confirmed that appropriate mechanical loading can optimize the ability of MSC-EVs to attenuate OA progression, providing a new idea for precise and minimally invasive treatment for OA.

Experimental section

Ethics statement

All animal operations were performed in strict accordance with the approval of the Animal Experiment Ethics

Committee of Hebei Medical University (Approval No. IACUC-Hebmu-2024016).

Cell preparation and identification

Human bone marrow-derived MSCs were purchased from Oricell™ (Cyagen Biosciences, China) and identified by multilineage differentiation assay and flow cytometry. For multilineage differentiation, MSCs were cultured in osteogenic, adipogenic, and chondrogenic induction media (Cyagen Biosciences) containing specific supplements. Following a 3-week culture period, Alizarin Red, Oil Red O, and Alcian Blue staining was carried out according to the manufacturer's instructions (Cyagen Biosciences). Flow cytometry analysis was then conducted to detect positive markers (CD90 and CD105) and negative marker (CD45) of MSCs using monoclonal antibodies (ThermoFisher, USA).

Primary chondrocytes were obtained from knee cartilage of 1-week-old C57BL/6 mice under sterile conditions as described previously.²² Briefly, articular cartilage tissue was isolated and minced into small fragments, and then digested with 0.25% trypsin-EDTA (Gibco, USA) for 15 min and 0.2% (m/v) type II collagenase (Solarbio Science & Technology, China) for 4 h. Then, the cartilage tissue was centrifuged and resuspended in DMEM (Gibco, USA) containing 10% fetal bovine serum (FBS; VivaCell Biosciences, China), and cultured in a cell incubator. The chondrocytes were subcultured when reaching 80% confluence. To prevent phenotypic loss, only second-generation chondrocytes were used in subsequent experiments.

Extraction of the MSC-EVs

A FlexCell bioreactor (Flexcell International Corporation, USA) was employed to form mechanical cyclic stretch for MSCs as previously demonstrated.^{23,24} MSCs were seeded into BioFlex six-well plates (Flexcell International Corporation, USA) with flexible silicone bottoms coated with collagen type I and cultured for 48 h. To extract the ML-EVs, BioFlex six-well plates were placed into the FlexCell bioreactor in which the MSCs were exposed to continuous cyclic sinusoidal tensile strain (8%, 1 Hz) for 6 h. The FlexCell bioreactor was incubated in the 37 °C incubator during the stretching. Meanwhile, the MSCs in the control group were only placed in the computer-regulated bioreactor without mechanical loading. Following mechanical loading, the culture medium was exchanged with serum-free DMEM and incubated for an additional 48 h. Subsequently, the conditioned medium was harvested for the isolation of EVs through ultracentrifugation. Specifically, the medium underwent centrifugation at 600g for 10 min, 2000g for 20 min, and 10,000g for 30 min to eliminate residual cells, debris, and large particles. The resulting supernatant was then subjected to ultracentrifugation twice at 110,000g for 75 min (Himac, Japan).

In addition, in order to extract EVs that overexpressed or knocked down miR-27b-3p, MSCs were transfected with miR-27b-3p mimics and miR-27b-3p inhibitors or the corresponding negative controls.²⁵ Then, the corresponding EVs were extracted and named miR-NC^{OE}-EVs, miR^{OE}-EVs, miR-NC^{KD}-EVs, and miR^{KD}-EVs, respectively.

Characterization of the MSC-EVs

The protein markers of the MSC-EVs (Alix, TSG101, CD63, and Calnexin) were analyzed via western blotting (Proteintech, China). MSC-EVs were observed and photographed via transmission electron microscopy (TEM, Hitachi, Japan). Moreover, nanoparticle tracking analysis (NTA, NanoFCM, China) was performed to detect the concentration and size distribution of the MSC-EVs.

Cellular uptake of MSC-EVs was also evaluated by labeling EVs with PKH67 dye (Sigma-Aldrich, PKH67GL). Briefly, 2 μ L of PKH67 dye was diluted in 200 μ L of Diluent C and then mixed with 200 μ L EVs. After incubation for 15 min in a cell incubator, 200 μ L FBS was added into the mixture to terminate reaction. PKH67-labeled EVs were ultracentrifuged and resuspended in 50 μ L PBS and then cocultured with chondrocytes for 8 h. Subsequently, the chondrocytes were fixed with 4% paraformaldehyde and dyed with DAPI, and photographed using a fluorescence microscope (Olympus BX51, Japan).

Mouse OA model and grouping

Twelve-week-old male C57BL/6 mice were chosen to establish a knee OA model via destabilization of the medial meniscus (DMM) surgery, as previously outlined.²² In brief, the mice were completely anesthetized by intraperitoneal injection of pentobarbital sodium. After hair removal and disinfection, a 0.5 cm longitudinal incision was made along the inside of the knee joint. The medial meniscus is exposed layer by layer, and a medial meniscotibial ligament is visible between the meniscus and the tibial plateau. Then, the medial meniscotibial ligament was incised to establish the DMM model. In the current study, the mice were divided into following groups: Sham, DMM + PBS, DMM + C-EVs, DMM + ML-EVs, DMM + miR-NC^{OE}-EVs, DMM + miR^{OE}-EVs, DMM + miR-NC^{KD}-EVs, DMM + miR^{KD}-EVs, DMM + CTP, and DMM + CTP/miR^{OE}-EVs ($n=5$). The sham group underwent only arthrotomy without injuring the meniscus. 10 μ L PBS or other therapeutic agents were administered via intra-articular injections to mice using a 33 g Hamilton microinjector once a week.

Micro-computed tomography analysis

About 6 weeks after DMM surgery, the mice were euthanized by an overdose intraperitoneal injection of sodium pentobarbital. The knee joints were isolated and fixed with 4% paraformaldehyde for 48 h. Then, the samples were

scanned with SkyScan 1174 μ CT scanner (Bruker, Luxembourg, Belgium). Subsequently, radiographic images were reconstructed via NRecon software (version 1.6, SkyScan), analyzed using CTAn software (version 1.9, SkyScan), and transferred to representative images of the 3D model using CTVol software (version 2.0, SkyScan).

Histological analysis

After fixation with 4% paraformaldehyde for 48 h, the samples were decalcified in EDTA decalcifying solution for a period of 3 weeks, dehydrated in a series of ethanol and xylene solutions, and subsequently embedded in paraffin. The paraffin-embedded specimens were then sectioned into 4 μ m-thick slices for the following experiments. Hematoxylin and eosin (HE) staining and safranin O-fast green (SO-FG) staining were conducted, and the Osteoarthritis Research Society International (OARSI) cartilage OA histopathology grading system was utilized to evaluate OA histopathology.²⁶ Moreover, immunohistochemical staining was carried out to detect the expression of biomarkers in the cartilage using anti-P16 (Abcam, catalog number: ab51243), anti-MMP13 (Proteintech, catalog number: 18165-1-AP), and anti-COLII (Proteintech, catalog number: 28459-1-AP) antibodies.

Cell immunofluorescence staining

After the corresponding treatments, chondrocytes were fixed, permeabilized, blocked, and then incubated with primary antibodies overnight at 4°C. Primary antibodies included anti-COLII (Proteintech, catalog number: 28459-1-AP), anti-MMP13 (Proteintech, catalog number: 18165-1-AP), and anti-P16 (Abcam, catalog number: ab51243) antibodies. Subsequently, chondrocytes were incubated with donkey anti-rabbit IgG (H + L) TRITC (Invitrogen, A16026; 1:500) and counterstained with DAPI (Beyotime, China) to stain the nuclei. Finally, chondrocytes were photographed using a fluorescence microscope (Olympus BX51) and analyzed through Image J software (Bethesda, MD, USA).

Senescence-associated β -galactosidase (SA- β -gal) staining

After corresponding treatments, the senescence of chondrocytes was detected using an SA- β -gal staining kit (Beyotime). Briefly, the chondrocytes were fixed with SA- β -gal fixative solution and incubated with SA- β -gal working solution overnight in a 37°C incubator. Senescent cells are stained blue under a microscope.

EdU staining assay

Chondrocytes were cultured in a 24-well plate (Corning, black, flat bottom) and cultured for 24 h. Following

the corresponding experimental treatments, chondrocytes were incubated with EdU working solution for 2 h according to the manufacturer's instructions (Beyotime). Chondrocytes were then fixed, permeabilized, and incubated with Click Additive Solution for 30 min in a cell incubator. Subsequently, we stained the nuclei with DAPI (Beyotime) for 10 min and obtained fluorescent images using a fluorescence microscopy (Olympus BX51).

Western blotting analysis

Chondrocyte proteins were extracted using radioimmuno-precipitation assay (Beyotime) lysis buffer supplemented with protease and phosphatase inhibitors. The concentration of these proteins was determined using a BCA Protein Assay Kit (Beyotime), and western blotting analysis was subsequently performed following an established protocol.²⁷ In brief, proteins were subjected to electrophoresis using SDS-PAGE (ACE biotechnology, China) and subsequently transferred to polyvinylidene difluoride membranes (EMD Millipore, USA). Following a 1 h incubation in 5% skim milk for blocking, the membranes were exposed to primary antibodies overnight, as detailed in Table S1. Subsequently, the membranes were treated with corresponding horseradish peroxidase-conjugated secondary antibodies (Proteintech) for 1 h. Protein bands were detected in an imaging system utilizing a ElectroChemiluminescence kit (Biosharp, China) and analyzed by Image J software (Bethesda).

EVs miRNA sequencing

The miRNA sequencing was carried out using RNA from C-EVs and ML-EVs by Sangon Biotechnology (China). The TruSeq Small RNA Sample Prep Kit (Illumina, USA) was utilized for library preparation, followed by sequencing on an Illumina HiSeq 2000/2500 with a read length of 50 bp. Subsequently, miRNA data analysis was performed via ACGT101-miR (v4.2).

Dual-luciferase reporter assay

The miRDB, TargetScan, and miRWalk bioinformatics web were used to predict the target genes of miR-27b-3p. In addition, miRDB was also used to predict the binding sites between miR-27b-3p and target genes. The dual-luciferase reporter assay was performed to verify target genes of miR-27b-3p. Wild-type ROR1 dual luciferase reporter vector (WT ROR1) and mutant ROR1 dual-luciferase reporter vector (MUT ROR1) were generated by Sangon Biotechnology (China). HEK293T cells were cultured in a 12-well plate at an appropriate density, followed by transfection with miR-27b-3p mimics and mimics NC along with the wild-type and mutant vectors. Luciferase activity was measured using a Dual-Luciferase Reporter Gene Assay Kit (Beyotime).

Transfection of siRNA

RNA interference can efficiently degrade specific mRNA and inhibit the expression of corresponding proteins. siRNA was synthesized by Sangon Biotechnology and transfected into chondrocytes using Lipofectamine 3000 (Beyotime) according to the product manual. The transfection effect was detected by WB experiment. The siRNA sequences of ROR1 were shown in Table S2.

Quantitative real-time PCR (qRT-PCR) analysis

Total RNA of MSCs, EVs, and chondrocytes was extracted using RZ Lysis Buffer (Tiangen, China). Then, cDNA was synthesized with a reverse transcription system, followed by qRT-PCR using SYBR Green PCR Master Mix (Tiangen). The $2^{-\Delta\Delta CT}$ method was employed to calculate the relative gene expression levels, with U6 serving as the internal control for normalizing the expression of miR-27b-3p. The specific primers were synthesized by Sangon Biotechnology and are as follows: U6 (F: 5'-CTCGCTTCGGCAGCAC-3', R: 5'-AACGCTTCACGAATTTGCGT-3'); miR-27b-3p (F: 5'-AATCGGCG TTCACAGTGGCTAA-3', R: 5'-ATCCAGTGCAGGGTCCGAGG-3').

Modification of EVs with CTP

CTP (DWRVIIPRPSA) was synthesized by GL Biochem (Shanghai, China). CTP was dissolved in 10 mM Tris (2-carboxyethyl) phosphine hydrochloride solution (MCE, HY-W011500) at a concentration of 1 mg/ml. DSPE-PEG-Maleimide (MCE, HY-140740) was dissolved at 1 mg/mL, and then mixed 1:1 with CTP solution and incubated at 4°C in darkness for 36 h. After another 24 h of dialysis, an appropriate amount of miR^{OE}-EVs was introduced and allowed to incubate at 4°C overnight. Finally, CTP-modified miR^{OE}-EVs (CTP/miR^{OE}-EVs) were obtained through ultracentrifuging at 110,000g for 75 min.

Metabolic kinetic of CTP/miR^{OE}-EVs in vivo

in vivo imaging system (IVIS) was employed to evaluate EVs metabolic kinetic *in vivo*. miR^{OE}-EVs and CTP/miR^{OE}-EVs were labeled with DiR (Cayman) and administered into the articular cavity. Subsequent *in vivo* imaging was conducted at 4, 24, 48, and 96 h after articular injection using the spectrum imaging system (PerkinElmer, Inc., America). Fluorescence intensity was analyzed to evaluate metabolic kinetic of miR^{OE}-EVs and CTP/miR^{OE}-EVs.

Statistical analysis

In this study, every experiment was repeated three times independently. GraphPad Prism V.8.0 software (San Diego, CA, USA) was employed to analyze the data. The

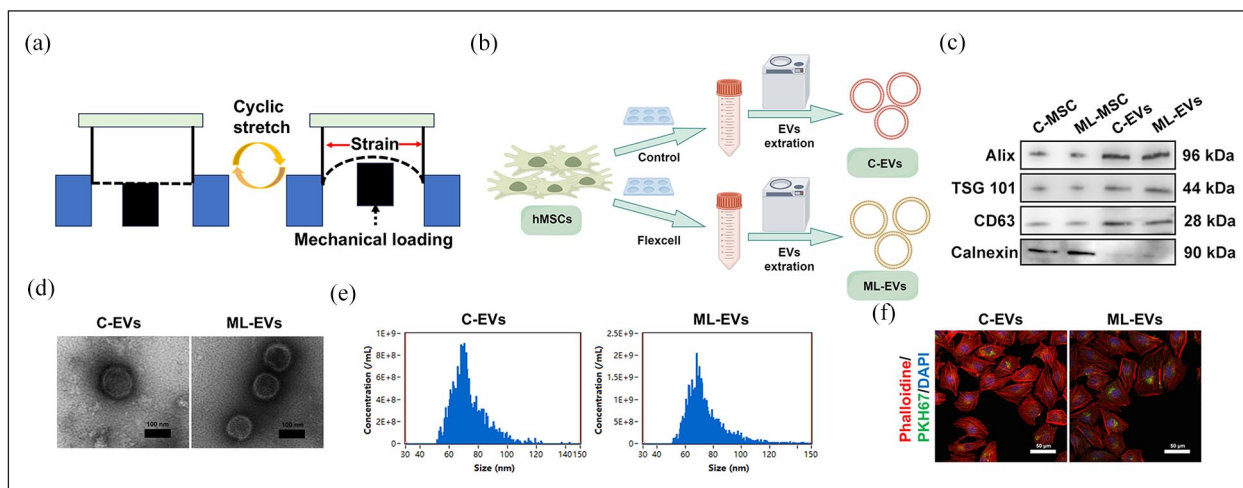


Figure 1. Identification and characterization of MSC-EVs. (a) Schematic diagram of mechanical loading treatment. (b) Flow diagram of the extraction of MSC-EVs. (c) Western blotting was performed to detect EVs-specific markers. (d) TEM images of MSC-EVs. Scale bar = 100 nm. (e) The diameter size distribution of MSC-EVs. (f) Internalization of MSC-EVs by chondrocytes. Scale bar = 50 μ m.

results are reported as the mean \pm standard deviations (SDs). Comparisons between two independent groups or multiple groups were conducted via Student's *t* test or one-way ANOVA, respectively. A *p* value <0.05 denoted a statistically significant distinction between the groups.

Results

Identification and characterization of MSCs and MSC-EVs

In light of the multidirectional differentiation potential of MSCs, a tri-lineage differentiation assay was conducted to evaluate their capacity to differentiate into osteogenic, chondrogenic, and adipogenic lineages. The differentiation potential was validated through Alizarin Red staining, Alcian Blue staining, and Oil Red O staining (Supplemental Figure S1A). Additionally, flow cytometry analysis revealed that MSCs expressed the surface markers CD105, CD90, and CD73, but lacked expression of CD45 (Supplemental Figure S1B).

MSCs were seeded into BioFlex six-well plates and subjected to continuous cyclic sinusoidal tensile strain. The schematic diagram of mechanical loading treatment was presented in Figure 1(a). MSC-EVs were extracted using the aforementioned methodology outlined in Figure 1(b). MSCs were exposed to continuous cyclic sinusoidal tensile strain (8%, 1 Hz) in the FlexCell bioreactor for 2, 6, 12, and 24 h. At the same time, the MSCs were exposed to continuous cyclic sinusoidal tensile strain (1 Hz) of different intensities (2%, 4%, 8%, or 12%) for 6 h. Then, the different ML-EVs were extracted and applied to treat chondrocytes exposed to TBHP (50 μ M). The

SA- β -gal assay indicated that ML-EVs extracted from MSCs subjected to 6 h and 8% continuous cyclic sinusoidal tensile strain presented the best anti-aging effect (Supplemental Figure S2A and S2B). Therefore, ML-EVs were extracted from MSCs exposed to continuous cyclic sinusoidal tensile strain (8%, 1 Hz) for 6 h.

Western blotting revealed significant differences in the expression of EV-specific markers (Alix, TSG101, CD63, and Calnexin) in both C-EVs and ML-EVs compared with that in MSCs, as depicted in Figure 1(c). TEM demonstrated the presence of a characteristic spherical bilayer membrane structure in both C-EVs and ML-EVs (Figure 1(d)). Furthermore, NTA revealed a similar size distribution of diameters between C-EVs and ML-EVs (73.2 ± 11.7 nm vs 74.5 ± 13.9 nm), as demonstrated in Figure 1(e). In addition, EVs uptake experiment indicated that C-EVs and ML-EVs could be endocytosed by chondrocytes (Figure 1(f)).

ML-EVs administration alleviated OA in comparison to C-EVs

Accumulating evidence has shown that MSC-EVs can mitigate OA progression. In order to evaluate the comparative efficacy of ML-EVs and C-EVs in the treatment of OA, we established a DMM mouse model, followed by intra-articular injection of C-EVs and ML-EVs (100 μ g/mL, once per week) over a period of 6 weeks (Figure 2(a)). As depicted in Figure 2(b) and (c), the micro-CT results of the knee joint presented an increased number of osteophytes in the DMM group, indicating successful induction of the OA model in mice. However, both C-EVs and ML-EVs obviously reduced osteophyte formation

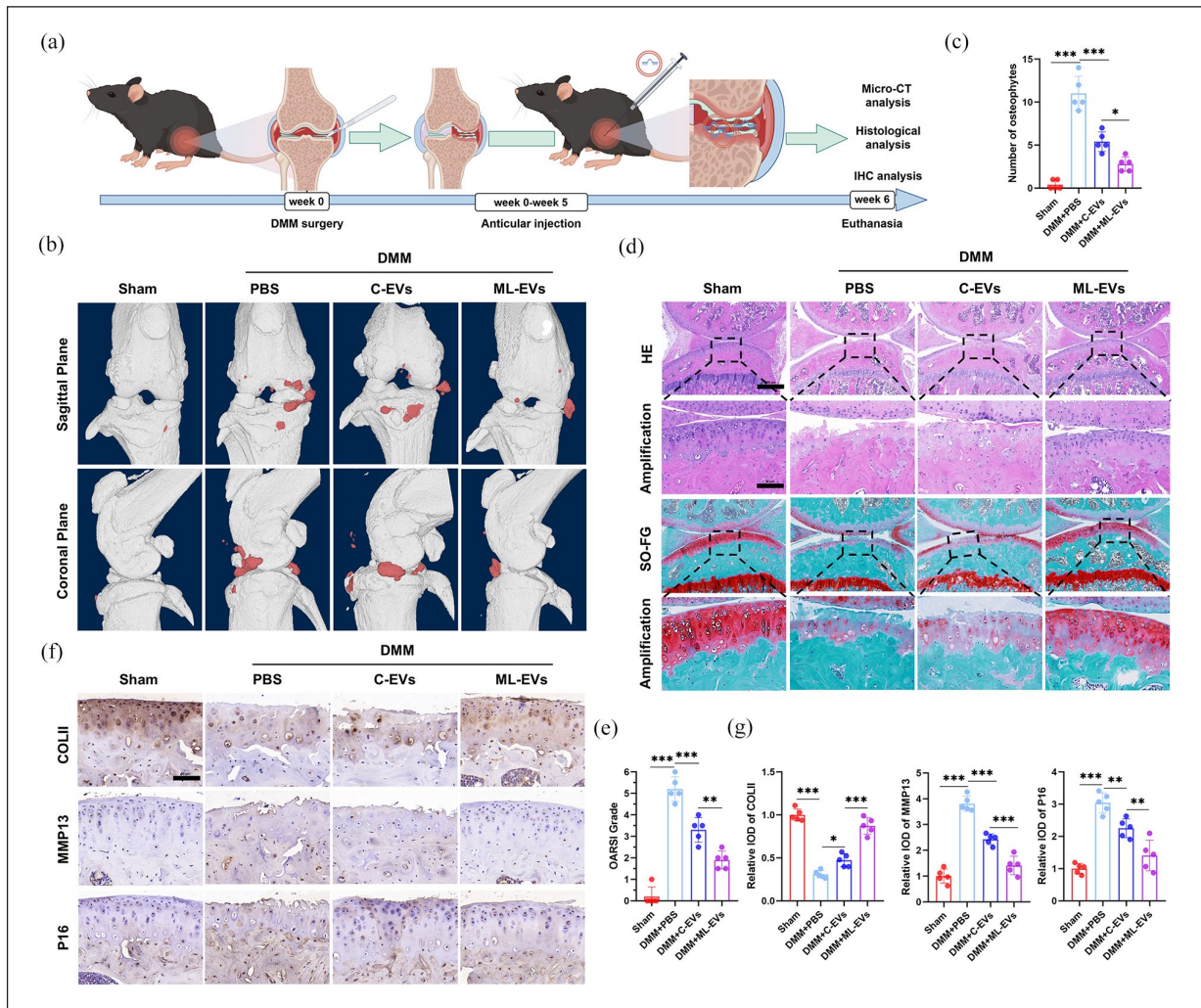


Figure 2. ML-EVs administration alleviated OA in comparison to C-EVs. (a) Schematic diagram of the in vivo administration of C-EVs and ML-EVs. (b) Representative 3D micro-CT images of frontal and lateral views of the knee joints. (c) Quantification of the number of osteophytes in each group. (d) Representative images of HE and SO-FG staining. Scale bar = 200 μ m. (e) Evaluation of the OARSI grade of each group. (f-g) Representative immunohistochemical images and quantification of COLII, MMP13, and P16 in the articular cartilage of each group. Scale bar = 50 μ m. $n = 5$.

Data were represented as the mean \pm SDs.

* $p < 0.05$. ** $p < 0.01$. *** $p < 0.001$.

induced by DMM surgery, with fewer osteophytes observed in the DMM + ML-EVs group than in the DMM + C-EVs group.

Consistent with the micro-CT results, HE and SO-FG staining showed that the DMM group exhibited a significant degenerative phenotype relative to the Sham group, characterized by a thin cartilage layer with an irregular morphological structure, a discontinuous and rough cartilage surface, and a decreased number of chondrocytes (Figure 2(d)). Although C-EVs significantly alleviated the OA degenerative phenotype, ML-EVs demonstrated superior therapeutic efficacy (Figure 2(e)). Additionally, immunohistochemical staining was conducted to assess the therapeutic effects of MSC-EVs in ameliorating ECM catabolism and chondrocyte senescence. Compared with those in the DMM group, the expression of the anabolic

biomarker (COLII) was elevated, whereas the levels of the catabolic molecule (MMP13) and the senescence biomarker (P16) were reduced following the administration of both C-EVs and ML-EVs (Figure 2(f) and (g)). Notably, alterations in the expression of these biomarkers were more pronounced with ML-EVs treatment. Overall, ML-EVs exerted more evident protective effects on attenuating OA progression than C-EVs.

ML-EVs administration ameliorated ECM degradation and chondrocyte senescence

To further substantiate the superior efficacy of ML-EVs over C-EVs in mitigating OA progression, we conducted an in vitro evaluation of their effects on cartilage ECM degradation and chondrocyte senescence. Chondrocytes

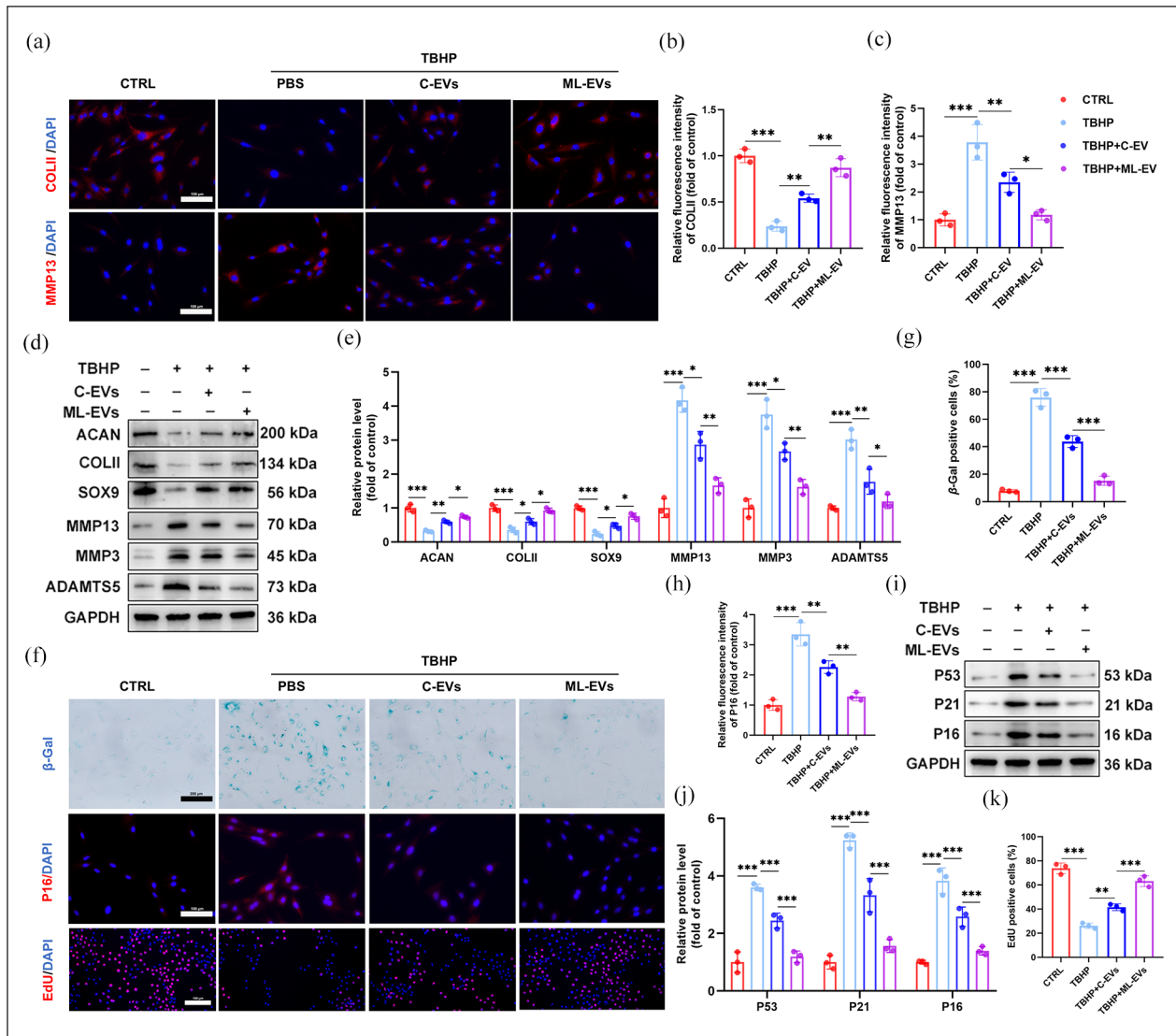


Figure 3. ML-EVs administration ameliorated ECM degradation and chondrocyte senescence. (a) Representative immunofluorescence images of COLII and MMP13 in chondrocytes. Scale bar = 100 μm. Quantification of COLII (b) and MMP13 (c) fluorescence intensity. (d–e) Representative western blotting images and quantification of the protein levels of ACAN, COLII, SOX9, MMP13, MMP3, and ADAMTS5 in chondrocytes. (f) Representative β-Gal staining images (Scale bar = 200 μm), immunofluorescence images of P16, and EdU staining images of chondrocytes (Scale bar = 100 μm). (g) Calculation of the percentage of β-Gal-positive chondrocytes. (h) Quantification of P16 fluorescence intensity. (i–j) Representative western blotting images and quantification of the protein levels of P53, P21, and P16 in chondrocytes. (k) Calculation of the percentage of EdU-positive chondrocytes.

Data were represented as the mean ± SDs from three independent experiments.

* $p < 0.05$. ** $p < 0.01$. *** $p < 0.001$.

were exposed to PBS, C-EVs (100 μg/mL), or ML-EVs (100 μg/mL) in the presence of TBHP (50 μM). As illustrated in Figure 3(a) to (c), MSC-EVs demonstrated the capacity to preserve ECM metabolic homeostasis, as evidenced by increased expression of COLII and decreased expression of MMP13. According to the western blotting results, both C-EVs and ML-EVs presented higher protein levels of anabolic markers (ACAN and COLII) and lower levels of catabolic markers (MMP13, MMP3, and ADAMTS5) than TBHP did (Figure 3(d) and (e)). Notably,

ML-EVs demonstrated a more pronounced effect on enhancing ECM anabolism and inhibiting catabolism.

Cellular senescence was also assessed to examine the therapeutic effects of EVs on OA. Both C-EVs and ML-EVs significantly attenuated TBHP-induced chondrocyte senescence, with ML-EVs showing superior anti-senescence effects, as evidenced by SA-β-gal assay (Figure 3(f) and (g)). As illustrated in Figure 3(f), immunofluorescence staining of P16 corroborated the functional role of the ML-EVs. Compared with those in

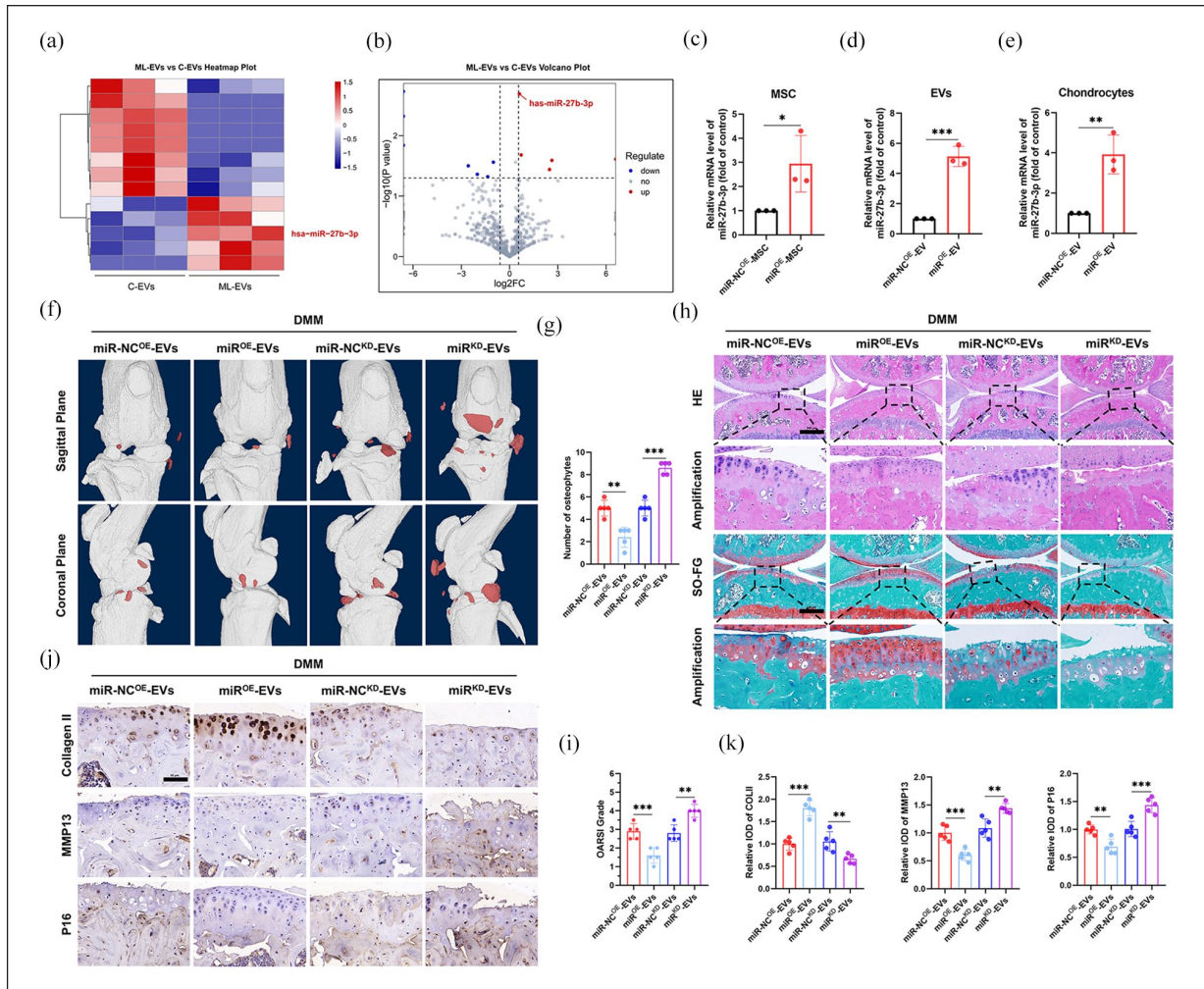


Figure 4. ML-EVs attenuated OA via delivery of miR-27b-3p in vivo. (a) Heatmap plot of the results of miRNA sequencing analysis. $n = 3$. (b) Volcano plot of the results of miRNA sequencing analysis. (c) Expression of miR-27b-3p in MSCs. (d) Expression of miR-27b-3p in EVs. (e) Expression of miR-27b-3p in chondrocytes. (f) Representative 3D micro-CT images of frontal and lateral views of the knee joints. (g) Quantification of the number of osteophytes in each group. (h) Representative images of HE and SO-FG staining. Scale bar = 200 μm . (i) Evaluation of the OARSI grade of each group. (j-k) Representative immunohistochemical images and quantification of COL11, MMP13, and P16 in the articular cartilage of each group. Scale bar = 50 μm . $n = 5$. Data were represented as the mean \pm SDs. * $p < 0.05$. ** $p < 0.01$. *** $p < 0.001$.

C-EVs, the protein levels of P53, P21, and P16 in the presence of ML-EVs were significantly lower (Figure 3(i) and (j)). Furthermore, the results of the EdU assay substantiated the preferential effect of ML-EVs in restoring the proliferative capacity of chondrocytes (Figure 3(k)). Collectively, these data revealed that ML-EVs could ameliorate ECM degradation and chondrocyte senescence, in accordance with the results of in vivo experiments.

miR-27b-3p was increased in ML-EVs and transferred to chondrocytes

Previous experiments, utilizing both in vitro and in vivo models, have demonstrated that ML-EVs exhibit superior

efficacy compared to C-EVs in mitigating ECM degradation, chondrocyte senescence, and the progression of OA. To further elucidate the mechanisms underlying the therapeutic benefits of ML-EVs, miRNA sequencing was performed on both C-EVs and ML-EVs. As illustrated in Figure 4(a) and (b), the heatmap and volcano plot revealed that five miRNAs were significantly upregulated (fold change ≥ 1.5 , $p < 0.05$) in the ML-EVs. Among these upregulated miRNAs, miR-27b-3p presented the highest expression level and was selected to investigate whether ML-EVs attenuate OA progression by delivering miR-27b-3p.

As previously described, MSCs were transfected with miR-27b-3p mimics and miR-27b-3p inhibitors, along

with their respective negative controls. Compared with that in MSCs transfected with the negative control, significant upregulation of miR-27b-3p expression was observed in MSCs transfected with the miR-27b-3p mimics (Figure 4(c)). Since the miR-27b-3p inhibitors function by binding to miR-27b-3p without affecting its synthesis, the effect of the inhibitors cannot be detected by PCR. Subsequently, miR-NC^{OE}-EVs, miR^{OE}-EVs, miR-NC^{KD}-EVs, and miR^{KD}-EVs were isolated from the corresponding MSCs. We characterized these EVs and found that their particle size and zeta potential were not significantly different from C-EVs (Figure S3). As illustrated in Figure 4(d), the level of miR-27b-3p was notably higher in the miR^{OE}-EVs than in the miR-NC^{OE}-EVs. Furthermore, the administration of miR^{OE}-EVs resulted in a significant increase in the miR-27b-3p level in chondrocytes compared with that in the miR-NC^{OE}-EVs-treated group (Figure 4(e)). In summary, mechanical loading substantially enhanced miR-27b-3p expression in ML-EVs, which can be delivered to chondrocytes.

ML-EVs alleviated OA through transporting miR-27b-3p in vivo

To ascertain the therapeutic efficacy of miR-27b-3p in the treatment of OA via ML-EVs, mice were subjected to DMM surgery, followed by the administration of miR-NC^{OE}-EVs, miR^{OE}-EVs, miR-NC^{KD}-EVs, and miR^{KD}-EVs. As depicted in Figure 4(f) and (g), micro-CT analysis revealed a substantial increase in osteophyte formation in the miR^{KD}-EVs group. Conversely, osteophyte formation was significantly impeded by miR^{OE}-EVs administration compared with that by miR-NC^{OE}-EVs administration, indicating that miR-27b-3p could alleviate OA progression in mice.

In accordance with the micro-CT results, HE and SO-FG staining showed a significant degenerative phenotype in the miR^{KD}-EVs group (Figure 4(h) and (i)). Notably, the administration of miR^{OE}-EVs markedly alleviated OA manifestations. Furthermore, immunohistochemical staining was performed to evaluate the therapeutic effects of miR-27b-3p. Compared to the miR-NC^{KD}-EVs group, the expression level of COLII reduced, while the levels of MMP13 and P16 elevated following treatment with miR^{KD}-EVs (Figure 4(j) and (k)). However, the administration of miR^{OE}-EVs reversed these changes, indicating that miR-27b-3p could maintain ECM homeostasis and hinder chondrocyte senescence.

ML-EVs administration protected chondrocytes through transporting miR-27b-3p in vitro

Given that ML-EVs mitigate OA progression by delivering miR-27b-3p in vivo, we proceeded to elucidate the underlying mechanisms via a series of in vitro experiments. Chondrocytes were exposed to miR-NC^{OE}-EVs, miR^{OE}-EVs, miR-NC^{KD}-EVs, or miR^{KD}-EVs in the presence of

TBHP (50 μ M). ECM metabolism was evaluated by immunofluorescence staining and western blotting of chondrocytes. As demonstrated in Figure 5(a) to (c), miR^{OE}-EVs treatment markedly increased the expression of the anabolic marker (COLII) and decreased that of the catabolic marker (MMP13) compared with miR-NC^{OE}-EVs treatment. Notably, the administration of miR^{KD}-EVs led to impaired ECM homeostasis relative to treatment with miR-NC^{KD}-EVs. Western blotting further corroborated that miR^{OE}-EVs could maintain ECM homeostasis (Figure 5(d) and (e)).

The SA- β -gal assay demonstrated that treatment with miR^{OE}-EVs resulted in a reduction in chondrocyte senescence (Figure 5(f) and (g)). However, the opposite results were observed with the miR^{KD}-EVs administration when compared with miR-NC^{KD}-EVs administration. Immunofluorescence staining of P16 further supported the anti-senescence effects of miR^{OE}-EVs (Figure 5(f), (h)). Additionally, the expression of P53, P21, and P16 decreased in chondrocytes treated with miR^{OE}-EVs but increased with miR^{KD}-EVs administration (Figure 5(i) and (j)). Furthermore, the results of the EdU assay confirmed the therapeutic effects of miR^{OE}-EVs in restoring the proliferative capacity of chondrocytes (Figure 5(k)). Taken together, these findings suggested that ML-EVs have the potential to mitigate ECM degradation and chondrocyte senescence through the delivery of miR-27b-3p in vitro.

miR-27b-3p suppressed the ROR1/NF- κ B signaling pathway

To further elucidate the molecular mechanism by which miR-27b-3p mitigates OA, we further explored target genes of miR-27b-3p in chondrocytes via the TargetScan, miRDB, and miRWalk databases. ROR1 was determined to be a potential target on account of its effect of promoting cartilage degeneration (Figure 6(a)). As shown in Figure 6(b), WT ROR1 and MUT ROR1 were established on the basis of the potential binding sites of miR-27b-3p. A dual-luciferase reporter assay indicated that the ROR1 3'-UTR is the direct target of miR-27b-3p (Figure 6(c)).

Further experiments were undertaken to elucidate the interaction between miR-27b-3p and ROR1. miR^{OE}-EVs significantly suppressed the expression of ROR1 in chondrocytes treated with TBHP (Figure 6(d) and (e)). Compared with miR-NC^{OE}-EVs, miR^{OE}-EVs markedly blocked the NF- κ B pathway, the downstream pathway of ROR1, in chondrocytes. Immunofluorescence staining of P65 also indicated that miR^{OE}-EVs impaired nuclear translocation of P65 induced by TBHP treatment (Figure 6(f)). Furthermore, we constructed siRNAs to knock down ROR1 in chondrocytes. Compared with siNC, siROR1-3 significantly reduced the protein level of ROR1, and thus, siROR1-3 was selected for subsequent experiments (Figure 6(g) and (h)). Moreover, the ROR1/NF- κ B pathway was significantly activated in the

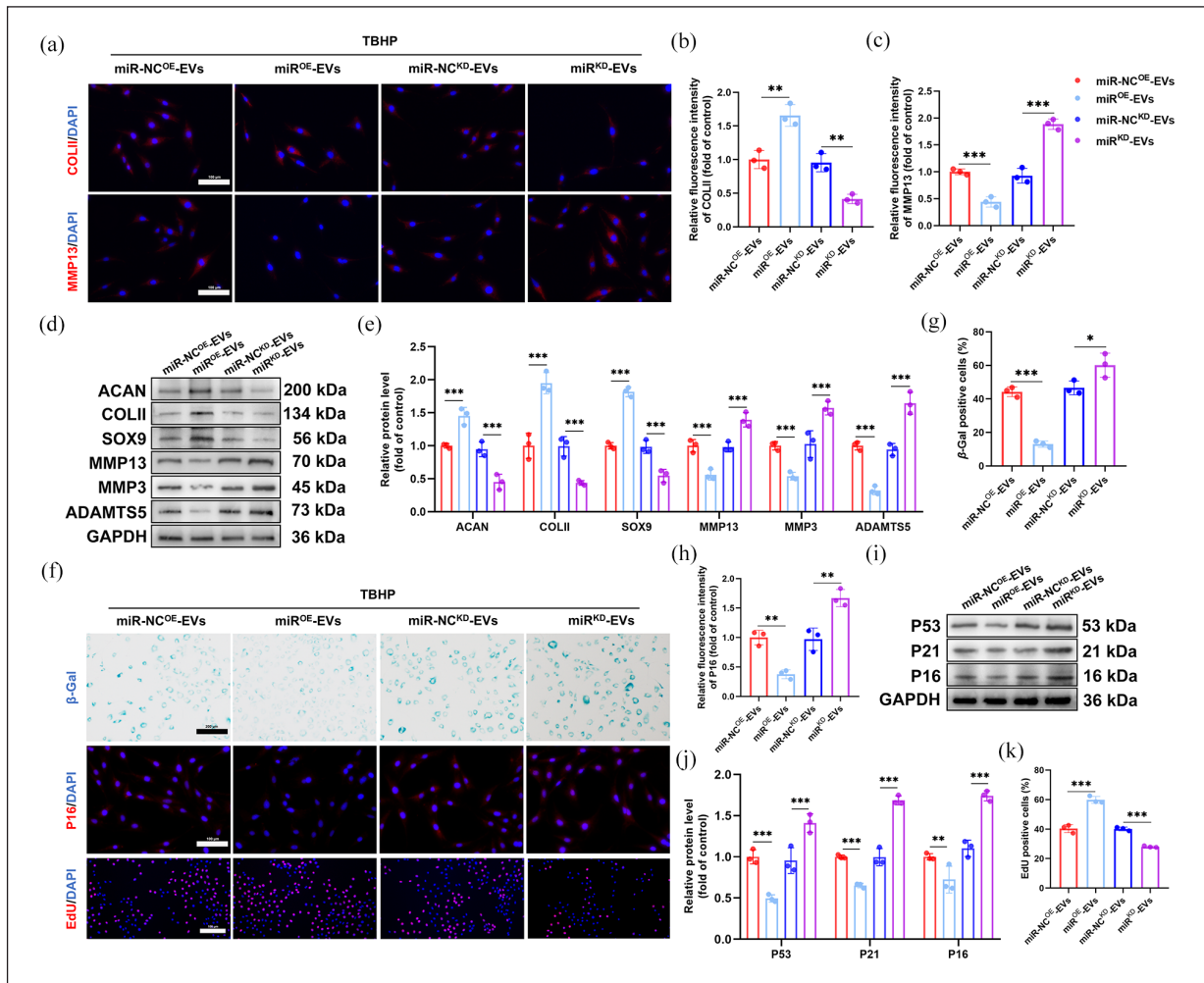


Figure 5. ML-EVs administration protected chondrocytes via delivery of miR-27b-3p in vitro. (a) Representative immunofluorescence images of COLII and MMP13 in chondrocytes. Scale bar = 100 μ m. Quantification of COLII (b) and MMP13 (c) fluorescence intensity. (d–e) Representative western blotting images and quantification of the protein levels of ACAN, COLII, SOX9, MMP3, and ADAMTS5 in chondrocytes. (f) Representative β -Gal staining images (Scale bar = 200 μ m), immunofluorescence images of P16, and EdU staining images of chondrocytes (Scale bar = 100 μ m). (g) Calculation of the percentage of β -Gal positive chondrocytes. (h) Quantification of P16 fluorescence intensity. (i–j) Representative western blotting images and quantification of the protein levels of P53, P21, and P16 in chondrocytes. (k) Calculation of the percentage of EdU-positive chondrocytes.

Data were represented as the mean \pm SDs from three independent experiments.

* p < 0.05. ** p < 0.01. *** p < 0.001.

miR^{KD}-EVs group compared with the miR-NC^{KD}-EVs group but was partially blocked by siROR1 (Figure 6(i) and (j)). Consistently, immunofluorescence staining of P65 revealed that siROR1 observably blocked nuclear translocation of P65 (Figure 6(k)). In summary, miR-27b-3p can inhibit the NF- κ B pathway in chondrocytes through targeting ROR1 (Figure 6(l)).

miR-27b-3p protected chondrocytes by targeting ROR1

Further experiments were conducted to determine whether miR-27b-3p can maintain ECM homeostasis and hinder chondrocyte senescence by targeting ROR1. Chondrocytes

were treated with miR-NC^{KD}-EVs, miR^{KD}-EVs, or miR^{KD}-EVs + siROR1 in the presence of TBHP (50 μ M). As depicted in Figure 7(a) to (c), immunofluorescence staining revealed that siROR1 restored matrix anabolism and inhibited matrix catabolism in chondrocytes. Western blotting analysis further confirmed that miR^{KD}-EVs + siROR1 exhibited a superior effect on maintaining ECM homeostasis compared with miR^{KD}-EVs alone (Figure 7(d) and (e)).

The SA- β -gal assay revealed a reduction in SA- β -gal positive chondrocytes following treatment with miR^{KD}-EVs + siROR1 compared with those following treatment with miR^{KD}-EVs alone (Figure 7(f) and (g)). Additionally, immunofluorescence staining of P16 provided further evidence of the anti-senescence properties of siROR1

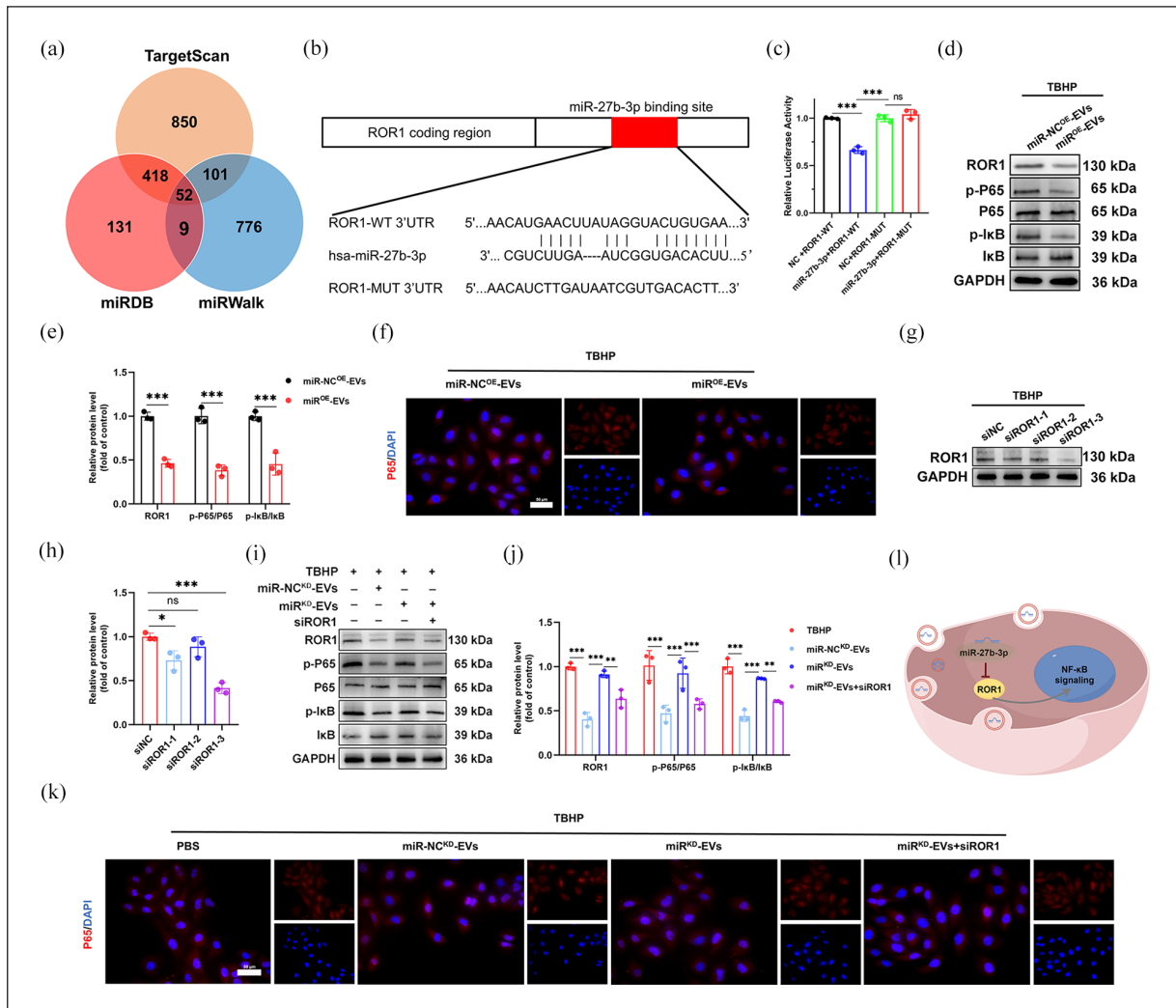


Figure 6. miR-27b-3p suppressed the ROR1/NF- κ B signaling pathway: (a) screening of target genes, (b) the binding site of miR-27b-3p in the target gene ROR1, (c) dual-luciferase reporter assay, (d–e) representative western blotting images and quantification of the protein levels of ROR1, p-P65, P65, p-I κ B, and I κ B in chondrocytes administered with miR-NC^{OE}-EVs or miR^{OE}-EVs, (f) immunofluorescence staining of P65 in chondrocytes administered with miR-NC^{OE}-EVs or miR^{OE}-EVs, (g–h) the protein level of ROR1 in chondrocytes treated with siNC or siROR1, (i–j) the protein levels of ROR1, p-P65, P65, p-I κ B, and I κ B in chondrocytes administered with miR-NC^{KD}-EVs, miR^{KD}-EVs, or siROR1 under the treatment of TBHP, (k) immunofluorescence staining of P65 in chondrocytes administered with miR-NC^{KD}-EVs, miR^{KD}-EVs, or siROR1 under the treatment of TBHP, and (l) schematic diagram of the mechanism by which miR-27b-3p targets ROR1 in chondrocytes.

Data were represented as the mean \pm SDs from three independent experiments.

* $p < 0.05$. ** $p < 0.01$. *** $p < 0.001$.

(Figure 7(f), (h)). Furthermore, the expression levels of P53, P21, and P16 were elevated in chondrocytes treated with miR^{KD}-EVs but were reduced upon siROR1 treatment (Figure 7(i) and (j)). Moreover, the results of the EdU assay further verified the therapeutic effects of siROR1 on restoring the proliferative properties of chondrocytes (Figure 7(k)). Together, these findings suggested that miR-27b-3p ameliorated ECM degradation and chondrocyte senescence by targeting ROR1.

Dual-engineered chondrocyte-targeted EVs attenuated OA in vivo

The above results indicated that ML-EVs are capable of preserving ECM homeostasis and mitigating chondrocyte senescence by delivering miR-27b-3p and modulating the ROR1/NF- κ B pathway, thereby decelerating OA progression. Consequently, we isolated miR^{OE}-EVs by transfecting MSCs with miR-27b-3p mimics. Given the

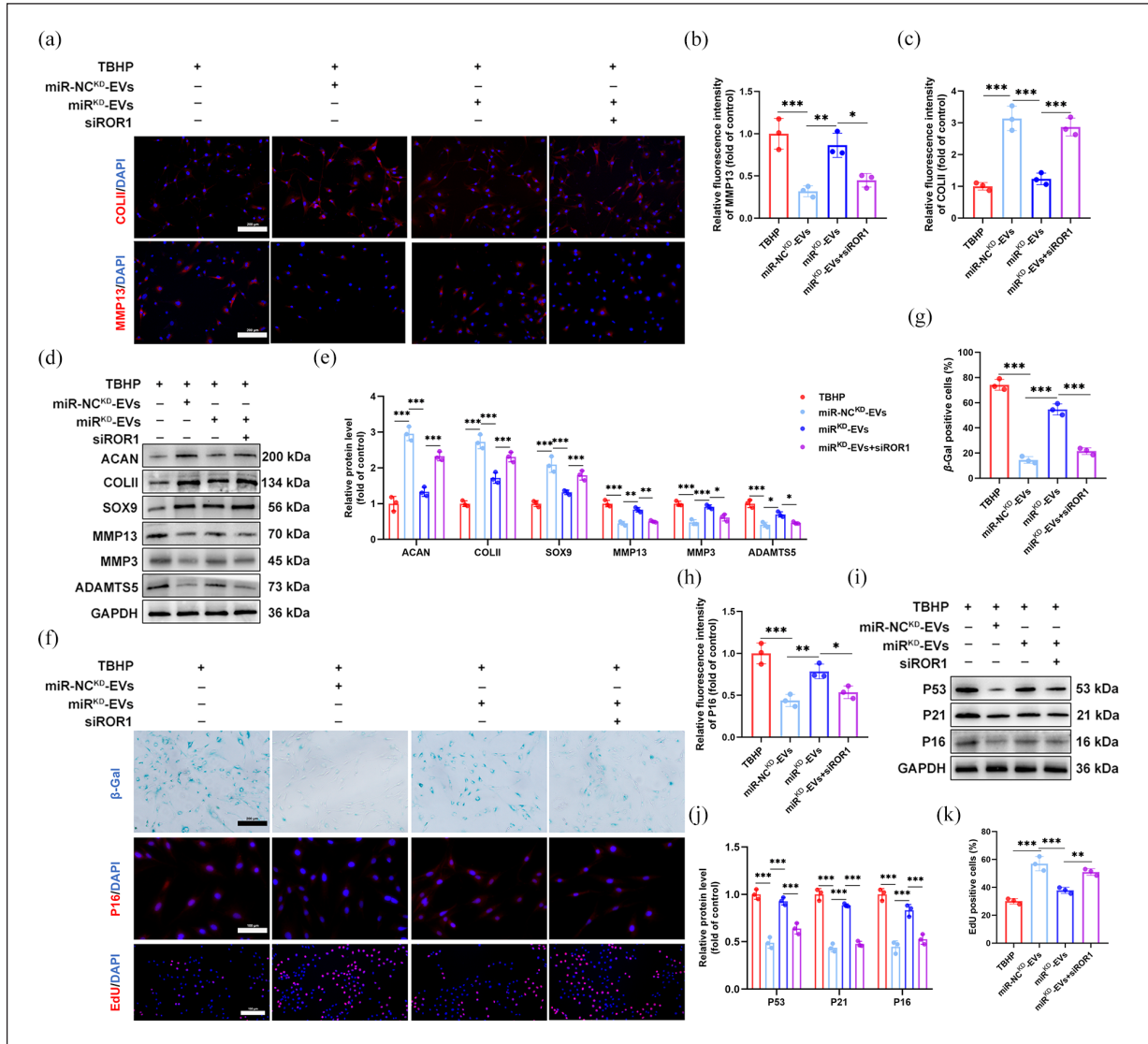


Figure 7. miR-27b-3p protected chondrocytes by targeting ROR1. (a) Representative immunofluorescence images of COL1I and MMP13 in chondrocytes. Scale bar = 100 μ m. Quantification of COL1I (b) and MMP13 (c) fluorescence intensity. (d–e) Representative western blotting images and quantification of the protein levels of ACAN, COLII, SOX9, MMP13, MMP3, and ADAMTS5 in chondrocytes. (f) Representative β -Gal staining images (Scale bar = 200 μ m), immunofluorescence images of PI6, and EdU staining images of chondrocytes (Scale bar = 100 μ m). (g) Calculation of the percentage of β -Gal-positive chondrocytes. (h) Quantification of PI6 fluorescence intensity. (i–j) Representative western blotting images and quantification of the protein levels of P53, P21, and P16 in chondrocytes. (k) Calculation of the percentage of EdU-positive chondrocytes. Data were represented as the mean \pm SDs from three independent experiments. * p < 0.05. ** p < 0.01. *** p < 0.001.

rapid clearance of EVs following intra-articular injection, strategies to enhance the chondrocyte-targeting efficacy of EVs within the articular cavity are imperative. Take into account the above reason, we enhanced the targeted delivery efficiency of miR^{OE}-EVs to chondrocytes by modifying miR^{OE}-EVs with CTP, named CTP/miR^{OE}-EVs (Figure 8(a)). The particle size and zeta potential of these EVs were characterized. The result indicated that and found that particle size and electrical potential of the

CTP/miR^{OE}-EVs increased slightly from miR^{OE}-EVs (Figure S4).

Flow cytometry was performed to verify whether CTP modification can improve the chondrocyte-targeting of miR^{OE}-EVs. Chondrocytes, osteoblast cell line MC3T3, and MSCs were labeled with DiI, DID, or DiI and DID, respectively. Then, miR^{OE}-EVs or CTP/miR^{OE}-EVs labeled with PKH-67 were administrated after mixing these cells (Figure 8(b)). Results of flow cytometry showed

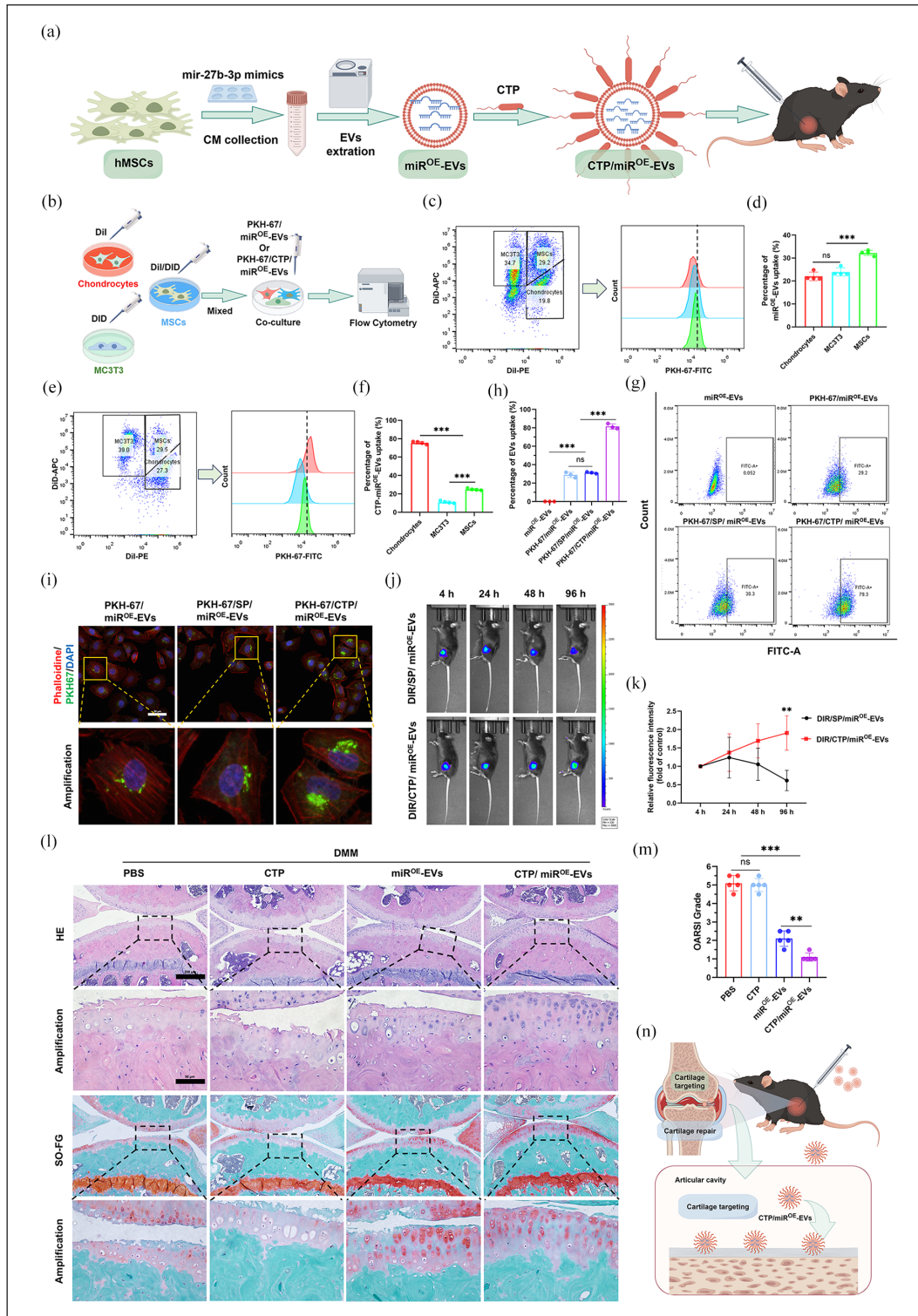


Figure 8. Dual-engineered chondrocyte-targeted EVs attenuated OA in vivo. (a) Flow diagram for the construction and application of CTP/miR^{OE}-EVs. (b) Schematic for assays evaluating the chondrocyte-targeting ability of CTP/miR^{OE}-EVs against miR^{OE}-EVs. miR^{OE}-EVs or CTP/miR^{OE}-EVs labeled with PKH-67 were administrated after labeling and mixing chondrocytes, MSCs, and MC3T3. (c–d) miR^{OE}-EVs uptake by chondrocytes, MSCs, and MC3T3 was evaluated by flow cytometry. (e–f) CTP/miR^{OE}-EVs uptake by chondrocytes, MSCs, and MC3T3 was evaluated by flow cytometry. (g–h) EVs uptake by chondrocytes was evaluated by flow cytometry. (i) Fluorescence image of the uptake of EVs by chondrocytes. (j–k) In vivo metabolic kinetic were detected with an IVIS. (l) Representative images of HE and SO-FG staining. Scale bar = 200 μm. (m) Evaluation of the OARSI grade of each group. (n) Schematic illustration of CTP/miR^{OE}-EVs targeting cartilage after entering the joint cavity.

Data were represented as the mean ± SDs.

* $p < 0.05$. ** $p < 0.01$. *** $p < 0.001$.

that MSCs uptake more PKH-67/EVs than that of chondrocytes and MC3T3, possibly due to the use of MSC-derived EVs or the more active metabolic activity of MSCs (Figure 8(c) and (d)). In addition, chondrocytes internalized the highest proportion of PKH-67/CTP/miR^{OE}-EVs among these cells, indicating that CTP modification increased the chondrocyte-targeting property of EVs (Figure 8(e) and (f)). Moreover, miR^{OE}-EVs were modified with randomly scrambled peptide (SP) and labeled with PKH-67, named PKH-67/SP/miR^{OE}-EVs. miR^{OE}-EVs, PKH-67/miR^{OE}-EVs, PKH-67/CTP/miR^{OE}-EVs, and PKH-67/SP/miR^{OE}-EVs were incubated with chondrocytes for 8 h to measure the uptake of EVs by chondrocytes. The results revealed no significant difference in internalization between the PKH-67/miR^{OE}-EVs and the PKH-67/SP/miR^{OE}-EVs (Figure 8(g) and (h)). However, the uptake of PKH-67/CTP/miR^{OE}-EVs by chondrocytes was significantly increased. Consistently, fluorescence microscopy also observed that the uptake of PKH-67/CTP/miR^{OE}-EVs by chondrocytes was significantly higher than that of other groups (Figure 8(i)).

Furthermore, to evaluate whether CTP modification can improve the delivery efficiency and sustainability of miR^{OE}-EVs in vivo, SP/miR^{OE}-EVs and CTP/miR^{OE}-EVs were labeled with DIR and injected into the articular cavity of mice. Fluorescence intensity was subsequently measured via IVIS. Although the EVs in both groups were not completely metabolized at 96 h, the fluorescence intensity in the SP/miR^{OE}-EVs group decreased significantly with time compared with that in the CTP/miR^{OE}-EVs group (Figure 8(j) and (k)). Notably, the fluorescence intensity of the CTP/miR^{OE}-EVs group gradually increased over time within 96 h, possibly due to targeted aggregation in the articular cartilage.

Furthermore, we established a DMM model to verify whether engineered EVs can play a superior role in delaying OA progression. After DMM surgery, the mice were administered with an equal volume of PBS, CTP, miR^{OE}-EVs, or CTP/miR^{OE}-EVs, respectively. HE and SO-FG results showed that miR^{OE}-EVs modified by CTP enhanced their protective effect on cartilage (Figure 8(l) and (m)). Overall, the modification of miR^{OE}-EVs optimized their ability to attenuate OA, owing to the increased chondrocyte-targeting ability and long-lasting effect duration of the engineered CTP/miR^{OE}-EVs (Figure 8(n)).

Discussion

The treatment of OA is a conundrum that has long plagued doctors and patients due to the lack of effective disease-modifying drugs.²⁸ The main pathology of OA is cartilage degeneration, mainly including ECM degradation and chondrocyte senescence and loss.³ MSCs and MSC-EVs have been proved to alleviate cartilage degeneration,

demonstrating promising therapeutic effects for OA.^{29–31} In this study, mechanical loading, a common form of physical stimulation, was shown to optimize the ability of MSC-EVs to maintain ECM homeostasis and inhibit chondrocyte senescence. Mechanistic exploration found that ML-EVs delivered miR-27b-3p to chondrocytes and inhibited the ROR1/NF- κ B axis. Further modification of EVs with CTP enhanced the ability of EVs to target chondrocytes and enhanced their ability to alleviate OA.

The primary pathological characteristic of OA is the gradual deterioration of articular cartilage function, which is attributed in part to the aging of chondrocytes and the resulting disruption of ECM metabolism.^{12,32} Our findings revealed that DMM surgery significantly reduced the thickness of the articular cartilage and the number of chondrocytes, while promoted ECM degradation and increased the proportion of senescent chondrocytes. MSC-EVs have been demonstrated to possess immunomodulatory effects and anti-inflammatory effects, as well as the ability to alleviate ECM metabolic disorders, thereby impeding cartilage deterioration.²⁹ Through targeting aging chondrocytes, MSC-EVs promote the repair of OA cartilage via delivery of miRNAs.⁶ In the current study, our results indicated that MSC-EVs alleviated TBHP-induced ECM metabolic disturbances and chondrocyte senescence. Furthermore, in vivo experiments revealed that MSC-EVs could reduce osteophyte formation, manifestation of cartilage degeneration, and the proportion of senescent chondrocytes.

Recently, researchers have continued to optimize the role of MSC-EVs in treating disease via engineering modifications, which overcome the limitations of natural MSC-EVs and improve their bioactivity and bioavailability, thereby amplifying their beneficial effects.³³ So far, multiple modification methods have been developed, including modification of MSC-EVs contents and the production environment and modification through combination with biomaterials.²⁹ For instance, hypoxic preconditioning has been demonstrated to enhance the effect of MSC-EVs on promoting chondrocyte proliferation, migration, and inhibiting apoptosis, in which miR-216a-5p plays a pivotal role.³⁴ In addition, mechanical loading has also been proved to promote the therapeutic effect of repairing cartilage by increasing the production of MSC-EVs.^{20,21} In the present study, we found that ML-EVs derived from mechanical loading primed MSCs demonstrated excellent ability to maintain matrix homeostasis and chondrocyte function. Furthermore, ML-EVs also significantly alleviated OA manifestations in vivo.

Among the therapeutic substances embedded within EVs, miRNAs have been demonstrated to be essential in the process of EVs-mediated cartilage repair.^{16,35,36} By pairing with the 3'-UTR of the target mRNA, miRNAs can regulate the function of chondrocytes via regulating the expression of post-transcriptional genes.³⁷ Accumulating

studies have revealed that miRNAs embedded in EVs can promote matrix synthesis and chondrocyte proliferation, and inhibit matrix degradation and chondrocyte senescence.^{6,38,39} Therefore, miRNA sequencing was performed to explore the effects of mechanical loading on miRNA expression in ML-EVs. miR-27b-3p was demonstrated to promote matrix homeostasis and chondrocyte proliferation, and impede chondrocyte senescence, thereby attenuating OA in vivo. Further mechanistic investigation revealed that miR-27b-3p works by targeting the ROR1/NF- κ B axis in chondrocytes.

The clinical treatment of OA with MSC-EVs still faces the challenges of poor drug delivery and poor targeting.⁴⁰ Researchers have reported that engineering modification of MSC-EVs effectively strengthened their targeting property toward the pathological sites, thereby improving delivery efficiency and therapeutic effectiveness.^{14,41} In this study, we also constructed a CTP that could target chondrocytes and modified it onto the membrane of MSC-EVs. In vitro experiments showed that CTP modification significantly increased the uptake of EVs by chondrocytes. Cao et al.⁶ revealed that modifying MSC-EVs with chondrocyte-targeted polymers enhanced their therapeutic efficiency and retention time in vivo. IVIS experiments revealed that CTP modification significantly increased the residence time of EVs in the joint cavity. Moreover, CTP modification significantly improved the ability of EVs to alleviate cartilage deterioration, matrix degradation, and chondrocyte senescence in OA.

Although our research proposed that mechanical loading optimized MSC-EVs for OA treatment and elucidated the underlying mechanism, several limitations remain to be resolved. First, we did not explore the effects of mechanical loading on MSC-EVs production or the specific mechanism involved. Second, frequent articular injections may bring some side effects, including pain, cartilage damage, and infection of the articular cavity. Therefore, a sustained-release system needs to be developed to achieve long-lasting therapeutic effects in MSC-EVs.

Conclusion

Mechanical loading preconditioning significantly optimized the ability of MSC-EVs to attenuate OA progression, mechanically through delivering miR-27b-3p and targeting the ROR1/NF- κ B axis. Dual-engineered EVs with overexpressed miR-27b-3p and chondrocyte-targeting properties demonstrated a maximal effect on alleviating OA.

Acknowledgements

We thank Jinglue Hu (Hebei Medical University, Shijiazhuang, China) for technical assistance in micro-CT scanning.

Author contributions

PW, HZ, and WC contributed equally to this work. PW: Conceptualization; Data curation; Investigation; Methodology; and Writing—original draft. HZ: Data curation; Formal analysis; and Writing—review & editing. WC: Supervision; Validation; and Writing—review & editing. YG: Investigation; Methodology; and Writing—original draft. SZ: Methodology; Project administration; and Writing—review & editing. XX: Resources; Software; and Project administration. SY and FW: Validation and Writing—review & editing. JW: Conceptualization; Funding acquisition; Supervision; and Writing—review & editing. ZS: Conceptualization; Supervision; and Writing—review & editing. YZ: Conceptualization; Funding acquisition; Supervision; and Writing—review & editing.

Data availability statement

All data needed to evaluate the conclusions in the paper are present in the paper and/or the Supplemental Materials. Additional data related to this paper are available from the authors upon reasonable request.

Declaration of conflicting interests

The author(s) declared no potential conflicts of interest with respect to the research, authorship, and/or publication of this article.

Funding

The author(s) disclosed receipt of the following financial support for the research, authorship, and/or publication of this article: This study was supported by the National Natural Science Foundation of China (Grant No. U23A6008; No. 91949203).

Ethical approval

All animal operations were performed in strict accordance with the approval of the Animal Experiment Ethics Committee of Hebei Medical University (Approval No. IACUC-Hebmu-2024016).

ORCID iD

Yingze Zhang  <https://orcid.org/0000-0003-2746-529X>

Supplemental material

Supplemental material for this article is available online.

References

1. Jeon OH, David N, Campisi J, et al. Senescent cells and osteoarthritis: a painful connection. *J Clin Invest* 2018; 128(4): 1229–1237.
2. Muthu S, Korpershoek JV, Novais EJ, et al. Failure of cartilage regeneration: emerging hypotheses and related therapeutic strategies. *Nat Rev Rheumatol* 2023; 19(7): 403–416.
3. Glyn-Jones S, Palmer AJ, Agricola R, et al. Osteoarthritis. *Lancet* 2015; 386(9991): 376–387.
4. Coryell PR, Diekmann BO and Loeser RF. Mechanisms and therapeutic implications of cellular senescence in osteoarthritis. *Nat Rev Rheumatol* 2021; 17(1): 47–57.

- Ji ML, Jiang H, Li Z, et al. Sirt6 attenuates chondrocyte senescence and osteoarthritis progression. *Nat Commun* 2022; 13(1): 7658.
- Cao H, Chen M, Cui X, et al. Cell-free osteoarthritis treatment with sustained-release of chondrocyte-targeting exosomes from umbilical cord-derived mesenchymal stem cells to rejuvenate aging chondrocytes. *ACS Nano* 2023; 17(14): 13358–13376.
- Wu X, Lai Y, Chen S, et al. Kindlin-2 preserves integrity of the articular cartilage to protect against osteoarthritis. *Nat Aging* 2022; 2(4): 332–347.
- Aicher WK, Bühring HJ, Hart M, et al. Regeneration of cartilage and bone by defined subsets of mesenchymal stromal cells—potential and pitfalls. *Adv Drug Deliv Rev* 2011; 63(4–5): 342–351.
- Brennan M, Layrolle P and Mooney DJ. Biomaterials functionalized with MSC secreted extracellular vesicles and soluble factors for tissue regeneration. *Adv Funct Mater* 2020; 30(37): 1909125.
- Jeong JO, Han JW, Kim JM, et al. Malignant tumor formation after transplantation of short-term cultured bone marrow mesenchymal stem cells in experimental myocardial infarction and diabetic neuropathy. *Circ Res* 2011; 108(11): 1340–1347.
- Woo CH, Kim HK, Jung GY, et al. Small extracellular vesicles from human adipose-derived stem cells attenuate cartilage degeneration. *J Extracell Vesicles* 2020; 9(1): 1735249.
- Boulestreau J, Maumus M, Jorgensen C, et al. Extracellular vesicles from mesenchymal stromal cells: therapeutic perspectives for targeting senescence in osteoarthritis. *Adv Drug Deliv Rev* 2021; 175: 113836.
- Hanai H, Hart DA, Jacob G, et al. Small extracellular vesicles derived from human adipose-derived mesenchymal stromal cells cultured in a new chemically-defined contaminate-free media exhibit enhanced biological and therapeutic effects on human chondrocytes in vitro and in a mouse osteoarthritis model. *J Extracell Vesicles* 2023; 12(7): e12337.
- Liang Y, Duan L, Lu J, et al. Engineering exosomes for targeted drug delivery. *Theranostics* 2021; 11(7): 3183–3195.
- Zhang S, Chu WC, Lai RC, et al. Exosomes derived from human embryonic mesenchymal stem cells promote osteochondral regeneration. *Osteoarthritis Cartilage* 2016; 24(12): 2135–2140.
- Lara-Barba E, Araya MJ, Hill CN, et al. Role of microRNA shuttled in small extracellular vesicles derived from mesenchymal stem/stromal cells for osteoarticular disease treatment. *Front Immunol* 2021; 12: 768771.
- Liu W, Liu A, Li X, et al. Dual-engineered cartilage-targeting extracellular vesicles derived from mesenchymal stem cells enhance osteoarthritis treatment via miR-223/NLRP3/pyroptosis axis: toward a precision therapy. *Bioact Mater* 2023; 30: 169–183.
- Phan J, Kumar P, Hao D, et al. Engineering mesenchymal stem cells to improve their exosome efficacy and yield for cell-free therapy. *J Extracell Vesicles* 2018; 7(1): 1522236.
- Sun Y, Ding SL, Zhao X, et al. Self-reinforced MOF-based Nanogel Alleviates Osteoarthritis by Long-acting Drug Release. *Adv Mater* 2024; 36(39): e2401094.
- Pang L, Jin H, Lu Z, et al. Treatment with mesenchymal stem cell-derived nanovesicle-containing gelatin methacryloyl hydrogels alleviates osteoarthritis by modulating chondrogenesis and macrophage polarization. *Adv Healthc Mater* 2023; 12(17): e2300315.
- Guo S, Debbi L, Zohar B, et al. Stimulating extracellular vesicles production from engineered tissues by mechanical forces. *Nano Lett* 2021; 21(6): 2497–2504.
- Yu H, Song Z, Yu J, et al. Supramolecular self-assembly of EGCG-selenomethionine nanodrug for treating osteoarthritis. *Bioact Mater* 2024; 32: 164–176.
- Chen Z, Zhao F, Liang C, et al. Silencing of miR-138-5p sensitizes bone anabolic action to mechanical stimuli. *Theranostics* 2020; 10(26): 12263–12278.
- Pu P, Wu S, Zhang K, et al. Mechanical force induces macrophage-derived exosomal UCHL3 promoting bone marrow mesenchymal stem cell osteogenesis by targeting SMAD1. *J Nanobiotechnology* 2023; 21(1): 88.
- Ma S, Xue R, Zhu H, et al. Selenomethionine preconditioned mesenchymal stem cells derived extracellular vesicles exert enhanced therapeutic efficacy in intervertebral disc degeneration. *Int Immunopharmacol* 2024; 132: 112028.
- Pritzker KP, Gay S, Jimenez SA, et al. Osteoarthritis cartilage histopathology: grading and staging. *Osteoarthritis Cartilage* 2006; 14(1): 13–29.
- Wang P, Zhang S, Liu W, et al. Bardoxolone methyl breaks the vicious cycle between M1 macrophages and senescent nucleus pulposus cells through the Nrf2/STING/NF- κ B pathway. *Int Immunopharmacol* 2024; 127: 111262.
- Cho Y, Jeong S, Kim H, et al. Disease-modifying therapeutic strategies in osteoarthritis: current status and future directions. *Exp Mol Med* 2021; 53(11): 1689–1696.
- You B, Zhou C and Yang Y. MSC-EVs alleviate osteoarthritis by regulating microenvironmental cells in the articular cavity and maintaining cartilage matrix homeostasis. *Ageing Res Rev* 2023; 85: 101864.
- Copp G, Robb KP and Viswanathan S. Culture-expanded mesenchymal stromal cell therapy: does it work in knee osteoarthritis? A pathway to clinical success. *Cell Mol Immunol* 2023; 20(6): 626–650.
- An X, Wang J, Xu K, et al. Perspectives on osteoarthritis treatment with mesenchymal stem cells and *Radix Achyranthis Bidentatae*. *Ageing Dis* 2024; 15(3): 1029–1045.
- Goldring SR and Goldring MB. Changes in the osteochondral unit during osteoarthritis: structure, function and cartilage-bone crosstalk. *Nat Rev Rheumatol* 2016; 12(11): 632–644.
- Komuro H, Aminova S, Lauro K, et al. Advances of engineered extracellular vesicles-based therapeutics strategy. *Sci Technol Adv Mater* 2022; 23(1): 655–681.
- Rong Y, Zhang J, Jiang D, et al. Hypoxic pretreatment of small extracellular vesicles mediates cartilage repair in osteoarthritis by delivering miR-216a-5p. *Acta Biomater* 2021; 122: 325–342.
- Foo JB, Looi QH, How CW, et al. Mesenchymal stem cell-derived exosomes and MicroRNAs in cartilage regeneration: biogenesis, efficacy, miRNA enrichment and delivery. *Pharmaceuticals (Basel)* 2021; 14(11): 1093.
- Qiu G, Zheng G, Ge M, et al. Mesenchymal stem cell-derived extracellular vesicles affect disease outcomes via transfer of microRNAs. *Stem Cell Res Ther* 2018; 9(1): 320.
- Bartel DP. MicroRNAs: genomics, biogenesis, mechanism, and function. *Cell* 2004; 116(2): 281–297.

38. Mao G, Zhang Z, Hu S, et al. Exosomes derived from miR-92a-3p-overexpressing human mesenchymal stem cells enhance chondrogenesis and suppress cartilage degradation via targeting WNT5A. *Stem Cell Res Ther* 2018; 9(1): 247.
39. Wang Z, Yan K, Ge G, et al. Exosomes derived from miR-155-5p-overexpressing synovial mesenchymal stem cells prevent osteoarthritis via enhancing proliferation and migration, attenuating apoptosis, and modulating extracellular matrix secretion in chondrocytes. *Cell Biol Toxicol* 2021; 37(1): 85–96.
40. Chen M, Lu Y, Liu Y, et al. Injectable microgels with hybrid exosomes of chondrocyte-targeted FGF18 gene-editing and self-renewable lubrication for osteoarthritis therapy. *Adv Mater* 2024; 36(16): e2312559.
41. Vader P, Mol EA, Pasterkamp G, et al. Extracellular vesicles for drug delivery. *Adv Drug Deliv Rev* 2016; 106(Part A): 148–156.